Journal of Fluids and Structures 53 (2015) 15–25

Contents lists available at ScienceDirect

Journal of Fluids and Structures

journal homepage: www.elsevier.com/locate/jfs

Feedback control of vortex shedding using a full-order optimal compensator

M. Carini [a], J.O. Pralits [b,*], P. Luchini [c]

[a] Dipartimento di Scienze e Tecnologie Aerospaziali, Politecnico di Milano (Campus Bovisa), via La Masa 34, 20156 Milano, Italy
[b] Dipartimento di Ingegneria Civile, Chimica e Ambientale, Università degli Studi di Genova, via Montallegro 1, 16145 Genova, Italy
[c] Dipartimento di Ingegneria Industriale, Università degli Studi di Salerno, via Ponte don Melillo 1, 84084 Fisciano (SA), Italy

ARTICLE INFO

Article history:
Received 9 October 2013
Accepted 30 November 2014
Available online 29 January 2015

Keywords:
Vortex shedding
Cylinder wake
Global instability
Optimal control

ABSTRACT

In the present study the linear feedback control of the unsteady cylinder wake is numerically investigated at low Reynolds numbers. The classical *small-gain* or *minimal control energy* (MCE) solution of the optimal control and estimation problems is used to design a full-dimensional stabilising compensator of the linearised Navier–Stokes equations, thus bypassing the open-loop model reduction of the fluid plant. For such high-dimensional system, both the feedback and the observer gains are efficiently computed based on the knowledge of the unstable global modes only. The derived control technique provides us with a theoretical analysis tool to investigate the best performance achievable by a 'perfect' MCE compensator, i.e. a MCE compensator free from model-reduction errors, on the actual flow field. In our setup, a *single-input-single-output* (SISO) configuration is considered, the vortex-shedding being controlled by means of the unsteady angular rotation of the cylinder surface with a single velocity sensor located in the wake for the state estimation. For $Re = 50$ the MCE compensator is able to completely suppress the cylinder vortex shedding, driving the flow from the natural limit cycle to the unstable basic state, which is finally restored. The effects of sensor placement on the compensator performance are then investigated and finally, as Re is increased, the upper bound on the delay of the instability threshold is assessed.

1. Introduction

The control of the vortex shedding occurring in the wake of a bluff body represents a great challenge for many engineering applications. The inherent low frequency unsteadiness of the flow field which results in higher aerodynamic loads, structural vibrations and acoustic noise, can indeed be significantly reduced by means of a suitable control action on the flow. A large number of investigations have been dedicated to this subject and various strategies have been proposed, as documented by the review of Choi et al. (2008). In particular, besides passive devices and open-loop techniques, active feedback controls have gained an increasing attention due to their ability to adapt to the actual flow conditions.

So far the flow past a circular cylinder has been established as a model problem for the understanding of bluff-body flow dynamics, thus becoming a classical topic in fluid mechanics. Several feedback control studies aimed at mitigating and suppressing the cylinder vortex shedding have been described in the past literature. In his experiments Roussopoulos (1993) was

* Corresponding author.
E-mail address: jan.pralits@unige.it (J.O. Pralits).

http://dx.doi.org/10.1016/j.jfluidstructs.2014.11.011
0889-9746/

able to delay the onset of the first instability of the cylinder wake up to $\mathrm{Re} \approx 58$. His control setup was comprised of a single hot-wire velocity sensor located in the wake, wall-mounted loudspeakers for the actuation and a phase shifter in the feedback control loop. A simple proportional feedback control has been numerically investigated by Park et al. (1994): in their simulations a single measurement of the flow vertical velocity on the symmetry line is used to drive a pair of synchronised blowing/suction slots located on the cylinder surface with an ad-hoc tuned feedback gain: different streamwise sensor positions are tested, achieving a complete suppression of the vortex shedding up to $\mathrm{Re} = 60$ for selected sensor locations.

During the past decade a model-based approach to flow control has been established within the framework of linear dynamical systems and optimal control theory (Kim and Bewely, 2007), with the *fluid plant* being derived from the linearised description of growing/decaying instabilities around the given basic state (Barbagallo et al., 2009; Ahuja and Rowley, 2010). Despite actual flow systems are highly nonlinear, for many flow configurations these linearised models are able to capture and describe the essential dynamics of developing flow instabilities, at least at their onset. At the same time, the linearised description allows for a systematic and rigorous approach to control design based on linear control theory, thus further motivating its application to flow control. Within this framework, the classical *Minimal Control Energy* (MCE) or *small-gain* solution of the Linear Quadratic Regulator (LQR) problem has been considered by Bewley et al. (2007) and more recently by Amodei and Buchot (2012) in view of its application to large-scale models of globally unstable flows derived from the numerical discretisation of the linearised Navier–Stokes equations. In particular, in both studies the MCE feedback rule of the full-order linearised flow model is efficiently computed based on the knowledge of the unstable left or *adjoint* eigenspace whose dimension is found to be small for typical fluid applications.

Until now only few authors have addressed the cylinder-wake stabilisation using linear optimal control theory. An example is provided in the paper by Protas (2004) where a Linear Quadratic Gaussian (LQG) compensator is designed based on a linearised Föppl-vortex model of the cylinder wake. More often optimal control theory has been exploited within a fully nonlinear framework based either on the Navier–Stokes equations (He et al., 2000; Protas and Styczek, 2002) or on nonlinear Reduced Order Models (ROMs) of the unsteady flow field (Bergmann et al., 2005), resulting in a *feedforward* control law to be applied to the flow in both cases.

In the present study the feedback control of the first instability of the cylinder wake is numerically investigated using linear optimal control. Starting from the work of Bewley et al. (2007), the small gain solution of the optimal estimation problem is also considered, leading to the design of a full-order LQG compensator in the so-called small-gain limit. This optimal control solution corresponds to what has been referred to as the "best control strategy" by Barbagallo et al. (2009). In that study concerning the feedback control of an open-cavity flow using balanced ROMs, the authors have shown that the performance of their reduced-order, small-gain compensator rapidly converges to the small-gain solution of the original control problem when the number of retained balanced modes is increased. From this point of view, the considered methodology provides us with a design tool to investigate the best performance achievable by such a reduced-order compensator when applied to a *flow oscillator* (Huerre and Rossi, 1998) and for a given plant configuration. In fact when a full-order approach is adopted, no approximations are introduced on the open-loop linearised dynamics, thus avoiding the so-called *spill-over* effects due to the undesired excitation of those stable dynamics which have not been retained in the open-loop ROM and which can affect the control action. With the same purpose, a more general and computationally demanding full-dimensional approach to the LQG design has been recently investigated by Semeraro et al. (2013) in the control of a two-dimensional boundary layer. In particular, the authors have shown that for such a highly convective system, when sensors are located downstream of the actuators, only a full-order compensator can always guarantees the stability of the closed-loop plant while varying the design parameters.

In our control setup of the cylinder wake, the control is performed by rotating the cylinder around its axis, with the related unsteady angular velocity being prescribed by the feedback rule as a function of time. Both the MCE-LQR controller and the MCE-LQG compensator are tested. In particular, when the compensator is employed, a single measurement of the cross-stream velocity component along the wake centreline is used for the state estimation. This sensor placement is mainly suggested by the symmetry-breaking nature of the flow instability with respect to the steady basic state. Furthermore in his experiments Roussopoulos (1993) has shown that away from the centreline, the unsteadiness caused by the vortex shedding is too weak to be used as a control signal. Finally, since only one unstable global mode exists for the considered flow, in principle effective feedback control can be achieved based on a single-sensor measurement only (Choi et al., 2008). Direct numerical simulations (DNS) are performed by applying the derived LQR and LQG control to the fully developed shedding cycle in order to assess the control effectiveness on the actual flow and to investigate its performance at increasing Reynolds number and for different streamwise locations of the sensor.

2. Problem definition and methodology

The two-dimensional flow past a circular cylinder is described using a Cartesian coordinate system with its origin located on the cylinder centre and with the x-axis aligned to the flow direction, as depicted in Fig. 1. The fluid motion is governed by the incompressible Navier–Stokes equations which are made dimensionless using the cylinder diameter $\tilde{D}$, the velocity of the incoming uniform stream $\tilde{V}_\infty$ and the constant density $\tilde{\rho}$:

$$\begin{cases} \dfrac{\partial \boldsymbol{V}}{\partial t} + (\boldsymbol{V}\cdot\nabla)\boldsymbol{V} = -\nabla p + \dfrac{1}{\mathrm{Re}}\nabla^2\boldsymbol{V}, \\ \nabla\cdot\boldsymbol{V} = 0, \end{cases} \tag{1}$$

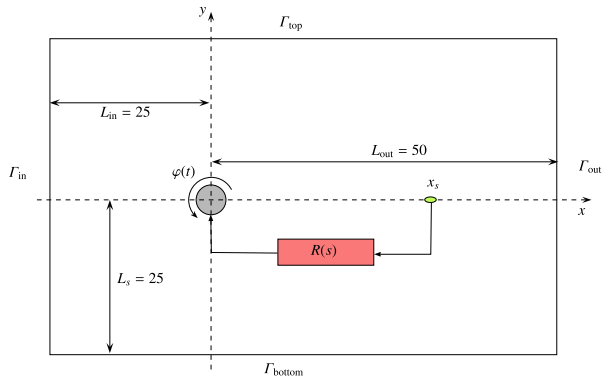

Fig. 1. Sketch of the computational domain Ω_c employed for numerical simulations of the flow past the circular cylinder with the adopted control setup. The localised cross-stream velocity measurement in the cylinder wake is fed back to the compensator $R(s)$ which drives the cylinder rotation.

where $\boldsymbol{V}$ denotes the velocity vector with components $\boldsymbol{V}=(U,V)$, P is the reduced pressure and $\mathrm{Re}=\tilde{V}_\infty\tilde{D}/\tilde{\nu}$ is the Reynolds number ($\tilde{\nu}$ being the kinematic viscosity of the fluid). In our control setup, the actuation is realised by means of unsteady angular rotations of the cylinder surface Γ_c around its axis, with $\varphi(t)$ denoting the unsteady cylinder angular velocity which is assumed positive in the counter-clockwise direction. Correspondingly, the boundary condition $\boldsymbol{V}=1/2\varphi\boldsymbol{\tau}$ is enforced on Γ_c, $\boldsymbol{\tau}$ being the unit tangent vector of Γ_c. At the same time localised velocity measurements in the wake are used to close the feedback loop.

The linear flow model for control design is derived almost straightforwardly from the linearisation of Eq. (1) around their steady solution for $\varphi=0$, i.e. the steady *base flow*. Once spatially discretised, the governing equations of the input–output linearised flow dynamics can be recast in the so-called *descriptor* form:

$$E\frac{d\boldsymbol{x}}{dt}=A\boldsymbol{x}+Bu, \tag{2a}$$

$$\boldsymbol{y}=C\boldsymbol{x}, \tag{2b}$$

where $\boldsymbol{x}$ denotes the vector of velocity and pressure states, $\boldsymbol{y}$ is the vector of wake velocity measurements and $u=\varphi$ is the control variable. In the above set of equations the operator $Ed(\cdot)/dt-A$ corresponds to the discrete counterpart of the linearised Navier–Stokes operator, with $E=E^T\geq 0$. It is well known from hydrodynamic stability theory that beyond the critical threshold of $\mathrm{Re}_{cr}\sim 47$ the flow past a circular cylinder becomes linearly unstable through a pair of complex-conjugate eigenmodes. The global modes ruling the flow stability properties and its open-loop dynamics are computed by solving the discrete generalised eigenvalue problem $A\hat{\boldsymbol{x}}=\lambda E\hat{\boldsymbol{x}}$ and its left or *adjoint* formulation $A^H\hat{\boldsymbol{p}}=\lambda^* E^H\hat{\boldsymbol{p}}$, where λ^* indicates the complex-conjugate of λ and $(\cdot)^H$ is employed here and in the following to denote the transpose-conjugate. The spatial structure of the direct and adjoint unstable global modes has been described by several authors both for a fixed cylinder (Giannetti and Luchini, 2007; Sipp and Lebedev, 2007; Marquet et al., 2008) and for a rotating cylinder at constant angular velocity (Pralits et al., 2010, 2013). The same results obtained in the former case will be used herein in order to design the stabilising small-gain LQG compensator of the considered flow.

2.1. The small-gain LQG compensator

Let us consider the stabilisable system $d\boldsymbol{x}/dt=A\boldsymbol{x}+B\boldsymbol{u}$ where A has no pure imaginary eigenvalues. It is a classical result of linear optimal control theory that when the small-gain limit is taken, the feedback rule $\boldsymbol{u}=K\boldsymbol{x}$ applied to the above system will result in the reflection of the unstable eigenvalues of A across the imaginary axis, while leaving unchanged all the remaining stable modes. For such control solution, the feedback gain matrix K can be computed by exploiting this particular structure of the closed-loop spectrum, which is known *a priori* (Lauga and Bewley, 2003). In particular, by means of projection of the state equations (2a) onto the unstable subspace (using adjoint modes) and transforming back to the original variables, the following expression for the MCE gain matrix K is derived (Lauga and Bewley, 2003; Bewley et al., 2007):

$$K=-R^{-1}B_u^H F^{-1}P_u^H E. \tag{3}$$

In the above formula, P_u is the matrix of the unstable left eigenvectors of the pencil (A,E), $B_u=P_u^H B$, and $R=R^H>0$ represents the control weight matrix of the infinite-horizon LQR cost function. The matrix F in (3) is simply defined as $F_{ij}=M_{ij}/(\lambda_{u,i}+\lambda_{u,j}^*)$ where $M=B_uR^{-1}B_u^H$ and $\lambda_{u,i}$ is the ith unstable eigenvalue of the pencil (A,E). Therefore, only the knowledge of the unstable adjoint global modes is required for the computation of K. Recently, this result has been extended by Amodei and Buchot (2012) to the case of a pencil (A,E) which is not diagonalisable with $E=E^T>0$.

In analogy with the regulator problem, the small-gain limit can be invoked also for the observer design within the classical framework of the *Kalman filtering* (Lewis and Syrmos, 1995; Burl, 1998). The linear observer which governs the

approximation $\boldsymbol{o}$ to the true state $\boldsymbol{x}$ in the presence of the state disturbance $\boldsymbol{d}$ and of the measurement noise $\boldsymbol{r}$ is defined as

$$E\frac{d\boldsymbol{o}}{dt} = A\boldsymbol{o} + B\boldsymbol{u} - L(\boldsymbol{y} - \boldsymbol{y}_o), \tag{4}$$

$$\boldsymbol{y}_o = C\boldsymbol{o}, \tag{5}$$

where L is the matrix of observer gains, also referred to as the *Kalman gain matrix*. In particular L can be equivalently computed as the solution of the infinite-horizon LQR problem for the so-called *dual* system of (2):

$$E^T\frac{d\boldsymbol{p}}{dt} = A^T\boldsymbol{p} + C^T\boldsymbol{n}, \tag{6}$$

where $\boldsymbol{n}$ indicates the dual fictitious control variable. The related cost function to be minimised is given by

$$J_e = 1/2\int_0^\infty \boldsymbol{p}^T W_{dd}\boldsymbol{p} + \boldsymbol{n}^T W_{rr}\boldsymbol{n}\, dt, \tag{7}$$

where the weight matrices W_{dd} and W_{rr} correspond to the covariance matrices of $\boldsymbol{d}$ and $\boldsymbol{r}$, respectively, with both disturbances being modelled as uncorrelated, zero mean, white Gaussian processes. Indeed this choice allows us to recover the original stochastic meaning of the Kalman filter within the deterministic formulation of the dual control problem. In particular, when the MCE or small-gain solution of the dual LQR control problem is considered, this corresponds to the Kalman filter design in the limit of $\ell^2 \to \infty$ with $\ell^2 = \|W_{rr}\|/\|W_{dd}\|$, i.e. in the limiting case of extremely noisy measurements compared to modelling errors on the state dynamics. Therefore the dual MCE solution can be referred to as the *maximum measurement noise* solution of the optimal estimation problem. The related gain matrix L can be computed by duality, where in the dual control problem C^H, W_{rr}, X_u and L^H play the same role as B, R, P_u and K, respectively, with X_u being used to denote the matrix of the unstable right (or *direct*) eigenvectors of the pencil (A,E). By substituting for the corresponding terms in (3), we arrive at the expression

$$L^H = -W_{rr}^{-1}C_u G^{-1} X_u^H E^H, \tag{8}$$

and then to

$$L = -EX_u G^{-H} C_u^H W_{rr}^{-1}, \tag{9}$$

where $C_u = CX_u$ and the matrix G is defined as $G_{ij} = N_{ij}/(\lambda_{u,i}^* + \lambda_{u,j})$ with $N = C_u^H W_{rr}^{-1} C_u$.

Once the small-gain limit is taken for both the control and the estimation problems, the small-gain LQG compensator is so derived. For such a compensator any control and estimation effort is focused on stabilising and estimating only the unstable modes of the uncontrolled system: this is emphasised by the right (left) multiplication by $P_u^H E$ (EX_u) in the definition of K (L). With reference to (3) and (8), the computation of both the feedback and the observer gain matrices require the knowledge of the unstable direct and adjoint global modes only. For typical fluid oscillators, such as bluff-body flows, the number of unstable modes is very small compared to the dimension of the discrete flow state, thus making the design of the considered compensator computationally feasible even for large-scale systems.

Although the control design is tackled directly at the discrete level, it is worthwhile to note that in the continuous setting and for a single control input, the linear *feedback operator* $\mathcal{K}(\cdot) \in \mathcal{L}(L^2(\Omega), \mathbb{R})$, which corresponds to the feedback gain matrix K (Curtain et al., 2007; Amodei and Buchot, 2012), can be expressed as

$$\varphi(t) = \mathcal{K}(\boldsymbol{v}) = \int_{\Omega_c} \boldsymbol{k}(x,y)\cdot\boldsymbol{v}(x,y,t)\, d\Omega_c, \tag{10}$$

where $\boldsymbol{v}(x,y,t)$ denotes the continuous linearised velocity field and $\boldsymbol{k}(x,y)$ is a two-dimensional vector field of feedback gains. The knowledge of $\boldsymbol{k}(x,y)$ provides a spatial representation of the feedback gains. Once the matrix K has been computed, a numerical approximation of $\boldsymbol{k}(x,y)$ can be obtained by means of a suitable discretisation of the above integral, according to the adopted discretisation of the flow equations, with

$$K\boldsymbol{x} = \sum_{i=1}^{N_w} \boldsymbol{v}(x_i,y_i)\boldsymbol{k}(x_i,y_i)w_i \approx \int_{\Omega_c} \boldsymbol{k}(x,y)\cdot\boldsymbol{v}(x,y,t)\, d\Omega_c, \tag{11}$$

where w_i denotes the quadrature weight associated with the ith quadrature node (x_i,y_i). Similarly, for the estimation problem using a single scalar measurement of the flow state, a continuous vector field $\boldsymbol{l}(x,y)$ can be introduced to describe the spatial distribution of the observer gains with

$$L(y - y_o) \approx \boldsymbol{l}(x,y)(y - y_o). \tag{12}$$

In this case the discrete approximation of $\boldsymbol{l}(x,y)$ follows straightforwardly from the adopted numerical discretisation of the flow equations, as for the direct global modes.

2.2. Numerical methods

The incompressible Navier–Stokes equations (1) and their linearised version are solved on the rectangular domain Ω_c which is illustrated in Fig. 1. In both cases the flow equations are discretised in conservative form on Cartesian smoothly varying staggered grids using standard second-order finite difference schemes. At the outlet boundary Γ_{out} the fully nonlinear equations are supplemented with the boundary conditions $-P+2\text{Re}^{-1}\partial U/\partial x=0$ and $\partial V/\partial x=0$. Both at the inlet Γ_{in} and at the side boundaries Γ_{top} and Γ_{bottom}, the vorticity is set to zero and the flow perturbation produced by the cylinder on the incoming uniform stream V_∞ is assumed to decay to zero as the leading term in the potential flow around it. For the linearised flow equations the above boundary conditions are applied with homogeneous data. An immersed boundary technique is employed to impose $\boldsymbol{V}=1/2\varphi\boldsymbol{\tau}$ on Γ_c (see Giannetti and Luchini, 2007, for details) while a bilinear interpolation is used to sample the velocity field at the selected sensor positions. Thus the non-zero entries of B and C are defined accordingly. Classical Newton iterations are used to compute the steady base flow while the leading global modes are extracted by means of the *Implicitly Restarted* Arnoldi method (Lehoucq et al., 1998). Time integration of the semi-discretised linear and nonlinear equations is performed making use of the hybrid Adams–Bashforth/Crank–Nicolson scheme: the diffusive terms and the pressure field are treated implicitly and at each time step a Stokes-like operator is numerically inverted using the sparse LU solver provided with the free software package UMFPACK (Davis, 2004). The same linear solver is employed to handle all other required matrix inversions in our computational setup. In the time integration of the closed-loop dynamics, both the control term $B\boldsymbol{u}(t)$ and the forcing term $L\boldsymbol{y}(t)$ are treated explicitly, thus resulting in a 'segregated' approach where the semi-discrete flow equations and the compensator are advanced in time separately, with a computational cost of $\sim$2 times the one associated with the uncontrolled flow simulation.

All the present results have been computed on a domain Ω_c of length $L_x=75$ in the streamwise direction and $L_y=50$ in the cross-stream direction. With reference to Fig. 1, the inlet, the outlet and the lateral boundaries are located at a distance from the origin equal to $L_{\text{in}}=25$, $L_{\text{out}}=50$ and $L_s=25$, respectively. The whole computational domain is discretised using 450×300 nodes with the grid points being clustered near the cylinder surface. More precisely, a uniform mesh with the finest grid spacing of $\Delta x=\Delta y=0.02$ is adopted within the small rectangular subdomain $[-1,1]\times[-1,1]$ enclosing the cylinder surface. Such grid will be referred to as M_0. In addition a finer mesh M_F with a similar structure was setup for convergence studies, consisting of 650×450 points with a minimum grid spacing of $\Delta x=\Delta y=0.01$. Finally for time integration, a non-dimensional step of $\Delta t=0.01$ is employed, which is reduced to $\Delta t=0.005$ when using the M_F grid. In order to validate the adopted spatio-temporal discretisation, computed DNS and stability results on both M_0 and M_F are reported in Table 1 along with the results obtained by different authors.

3. Results

It is well known that when the Reynolds number is increased beyond the critical value of $\text{Re}_{\text{cr}}\sim47$, the steady base flow around a circular cylinder becomes linearly unstable with a pair of complex-conjugate global modes. The computed unstable eigenvalues λ_u along with the base flow drag coefficient $C_D^{(BF)}$ are reported in Table 2 for $\text{Re}=50, 70$ and 90. For these values of Re the two-dimensional vector gain-field $\boldsymbol{k}(x,y)$ corresponding to the computed gain matrix K is illustrated in Fig. 2 (left column). In agreement with the prior results of Bewley et al. (2007), the modulus of $\boldsymbol{k}(x,y)$ is sharply localised close to the cylinder surface and its spatial pattern is found very similar to that of the unstable adjoint global mode of the cylinder wake (Giannetti and Luchini, 2007; Marquet et al., 2008), although the gain field does not exactly correspond to the adjoint field. Indeed it can be shown from Eq. (3) that, in the present case, K results from a linear combination of the real and imaginary part of the unstable left eigenvector $\hat{\boldsymbol{p}}_u$:

$$K=\gamma_r\Re(\hat{\boldsymbol{p}}_u)+\gamma_i\Im(\hat{\boldsymbol{p}}_u), \tag{13}$$

with γ_r and γ_i being two real valued coefficients. High values of the feedback gain field are located in the regions of maximum amplitude of the unstable adjoint mode where, by definition, the corresponding direct mode can be easily

Table 1
Comparison of DNS and linear global stability results for the flow past a rotating and a fixed cylinder, respectively, with the corresponding values obtained by different authors. Results computed on both the standard grid $M0$ (450×300) and the refined grid M_F (650×450) are reported. With reference to DNS results, St is the Strouhal number while C_L and C_D are the lift and drag coefficients, respectively. The symbol $\langle\cdot\rangle$ denotes time averaged quantities while the prime indicates the amplitude of the fluctuations around the mean value. For the global stability analysis, both the critical Reynolds number Re_{cr} and the critical frequency ω_{cr} associated with the marginally stable global mode are reported.

Refs.	DNS at $\text{Re}=100$, $\lvert\varphi\rvert=2$					Global stability	
	$\langle C_D\rangle$	$\lvert\langle C_L\rangle\rvert$	C_D'	C_L'	St	Re_{cr}	$\omega_{\text{cr}}/(2\pi)$
M_0 (Present)	1.1052	2.4957	0.101	0.3554	0.1656	46.53	0.1165
M_F (Present)	1.1021	2.4996	0.102	0.3575	0.1656	46.64	0.1165
Kang et al. (1999)	1.1040	2.4881	0.0993	0.3631	0.1655	–	–
Stojković et al. (2002)	1.1080	2.504	0.0986	0.3616	0.1658	–	–
Giannetti and Luchini (2007)	–	–	–	–	–	46.7	0.118
Meliga and Chomaz (2011)	–	–	–	–	–	46.7	0.116

Table 2
Steady base flow past a fixed circular cylinder: computed unstable eigenvalues λ_u and drag coefficient $C_D^{(BF)}$ for three different values of Re.

Data	Re = 50	Re = 70	Re = 90
λ_u	0.0139 ± 0.736i	0.0737 ± 0.744i	0.110 ± 0.734i
$C_D^{(BF)}$	1.3808	1.2142	1.1058

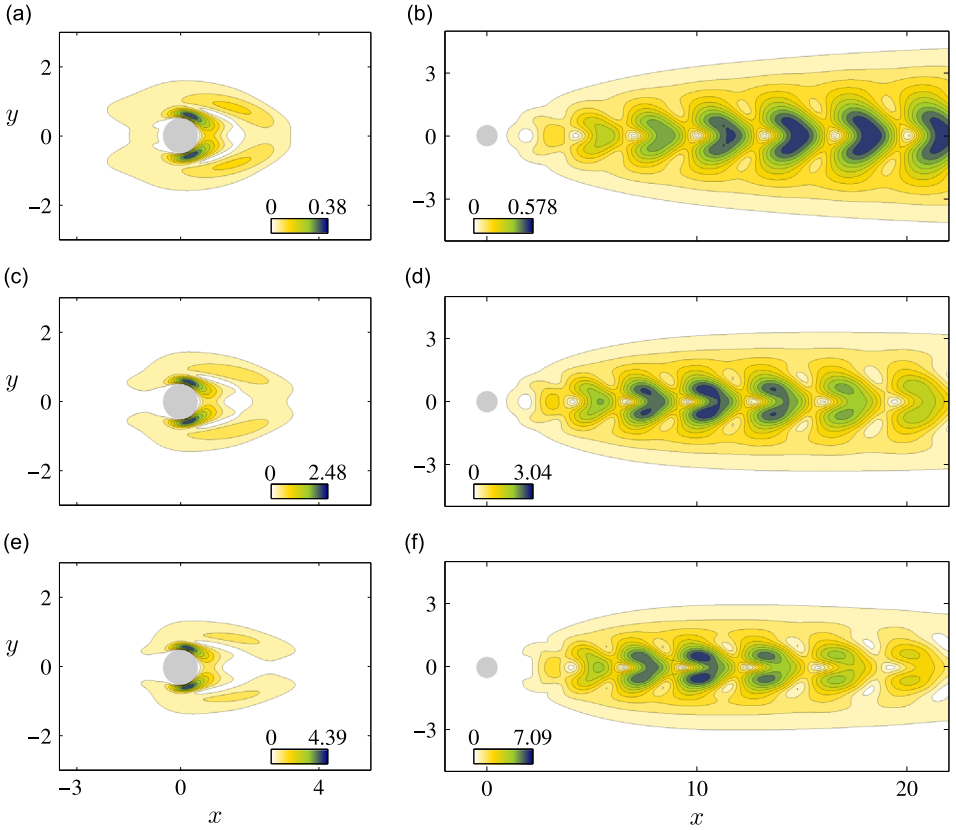

Fig. 2. Computed feedback and observer gain fields for various Reynolds numbers: $\|\boldsymbol{k}(x,y)\|$ (left column) and $\|\boldsymbol{l}(x,y)\|$ associated with a single cross-stream velocity sensor located at $(x,y)=(1.0,0.0)$ (right column). (a,b) Re = 50. (c,d) Re = 70. (e,f) Re = 90.

excited. At increasing Reynolds number these regions gradually shrink as shown by Giannetti and Luchini (2007) for the maxima of the adjoint global mode field.

Similar considerations also hold for the Kalman gain matrix L that has been computed with reference to a single sensor of the cross-stream velocity component located at $(x_s, y_s) = (1, 0)$. The spatial distribution of the observer gains is illustrated in Fig. 2 (right column) by showing the modulus of the associated vector field $\boldsymbol{l}(x,y)$. In a dual manner with respect to $\boldsymbol{k}$, the pattern of $\boldsymbol{l}$ is found very similar to that of the direct unstable global mode, with L resulting from the linear combination of the real and imaginary part of the unstable right eigenvector $\hat{\boldsymbol{x}}_u$. Correspondingly, gain maxima are located in the far wake region, along the symmetry line, where the global mode is most easily observable, and gradually move upstream as the Re is increased. With reference to Eqs. (3) and (8), it can be noticed that in the considered SISO case, the numerical values of R and W_{rr} do not affect the gain values, therefore both R and W_{rr} are assumed equal to 1. The computed solutions for K and L have been validated on the linearised flow system by evaluating both the growth-rate and the frequency of the least stable modes of $A+BK$ and $A+LC$, respectively, which indeed correspond to the reflected unstable eigenvalues of A in both cases.

The effectiveness of the proposed control strategy is now assessed on the nonlinear flow at Re = 50. Starting from the fully developed shedding cycle, both the full-information controller and the SISO compensator are shown to be able to drive the flow towards the unstable basic state which is finally restored. This is clearly illustrated in Fig. 3 by means of the time traces of the aerodynamic force coefficients: both C_D and C_L converge to the constant values which characterise the base-flow solution with C_D=1.3808 and C_L=0. The corresponding control signal, i.e. the cylinder angular velocity $\varphi(t)$ is also illustrated in Fig. 3(d), where $\varphi(t)$ asymptotically goes to zero. In these pictures as well as in the following ones, the

non-dimensional time t has been rescaled on the Strouhal number St of the uncontrolled periodic flow, thus providing a measure of the time required to suppress the vortex shedding in terms of the equivalent number of natural shedding cycles. For both the full-information controller and the compensator, the control forcing is activated at the same time instant

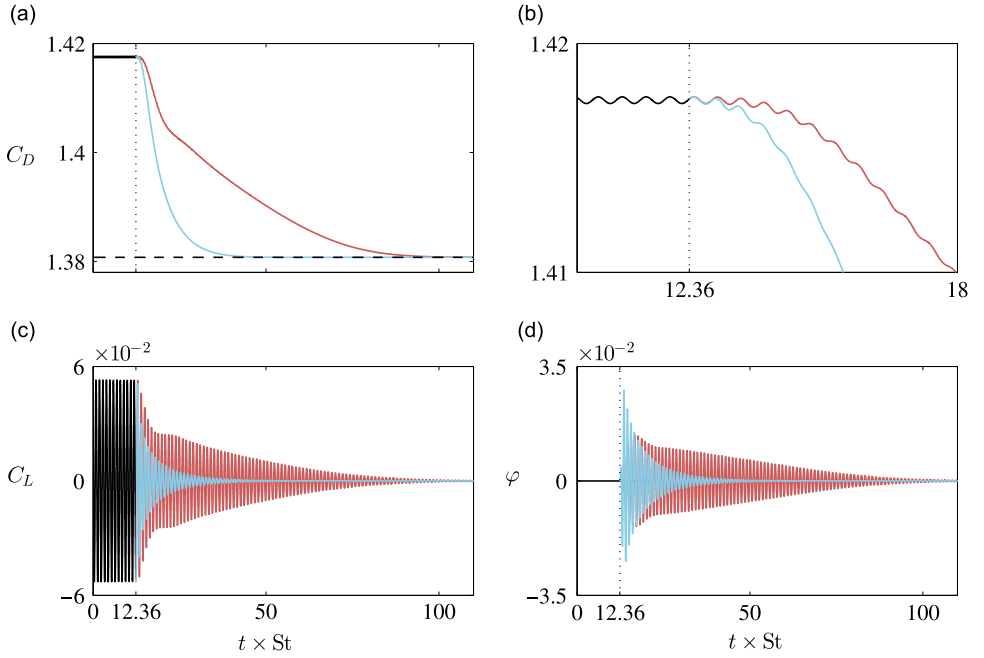

Fig. 3. Control of the flow past a circular cylinder at Re = 50: full-information control (blue line) and SISO compensator fed by a single cross-wise velocity sensor located at $(x_s, y_s) = (1.0, 0)$ (red line). Control is applied to the fully developed limit cycle (black line) starting from $t \times \mathrm{St} \approx 12.36$. (a) Drag coefficient $C_D(t)$. (b) Detailed view of $C_D(t)$ when control is activated. (c) Lift coefficient $C_L(t)$. (d) Cylinder angular velocity $\varphi(t)$. The horizontal dashed line in (a,b) denotes the value of $C_D^{(BF)}$. (For interpretation of the references to color in this figure caption, the reader is referred to the web version of this article.)

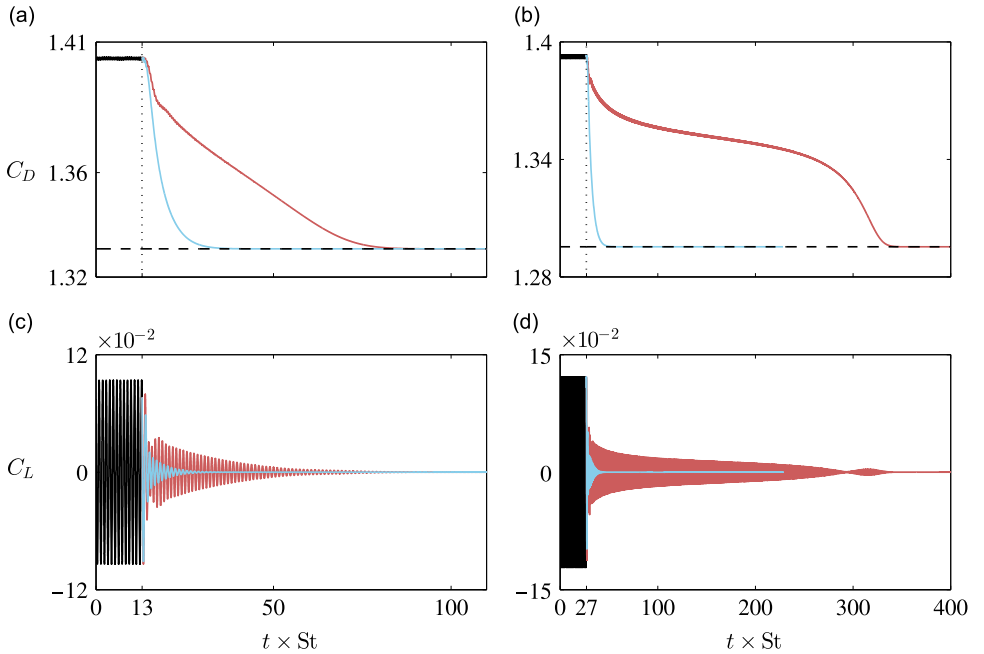

Fig. 4. Control of the flow past a circular cylinder at Re = 55 (left panels) and at Re = 59 (right panels): full-information controller (blue line) and the SISO compensator (red line), the sensor being located at $(x_s, y_s) = (2.0, 0)$. Control is applied to the fully developed limit cycle (black line) starting at $t \times \mathrm{St} \approx 13$ and $t \times \mathrm{St} \approx 27$ for Re = 55 and Re = 59, respectively. (a,b) Drag coefficient $C_D(t)$; the horizontal dashed line indicates the value of $C_D^{(BF)}$ for the considered Reynolds number. (c,d) Lift coefficient $C_L(t)$. (For interpretation of the references to color in this figure caption, the reader is referred to the web version of this article.)

($t_s \times \mathrm{St} \approx 12.36$) and smoothly applied to the cylinder by means of a blended step function $H_b(t)$, i.e. $\varphi(t)H_b(t-t_s)$ where

$$H_b(t) = \begin{cases} \frac{1}{2}\left(1-\cos\left(\pi t/\Delta t_c\right)\right), & \text{for } t < \Delta t_c \\ 1, & \text{for } t \geq \Delta t_c, \end{cases} \tag{14}$$

with Δt_c indicating the time-window size of the blended step which has been fixed to $\Delta t_s = 10$ in all our simulations. As expected, the full-information controller performs better than the compensator by achieving flow stabilisation over a shorter time window ($\sim$40 cycles) compared to the second ($\sim$100 cycles). Indeed for the compensator a certain amount of time is spent for state estimation and only once a suitable linear estimate of the flow has been obtained, the control becomes effective. By increasing the Reynolds number, the amount of time needed by the compensator to stabilise the flow also increases. This is well illustrated in Fig. 4 by comparing the performance of the compensator with respect to that of full-information controller for $\mathrm{Re} = 55$ and $\mathrm{Re} = 59$, the velocity sensor being located at $(x_s, y_s) = (2.0, 0.0)$ in both cases. For $\mathrm{Re} = 59$ the MCE compensator takes $\sim$300 shedding cycles to completely suppress the vortex shedding while the performance of the full-information control results substantially unchanged. As will be shown in the following section, for $\mathrm{Re} > 59$ the MCE compensator is not able to stabilise the flow anymore.

3.1. Sensitivity to sensor placement and Reynolds number

The sensitivity of the compensator performance to different streamwise locations x_s of the sensor has been investigated, similar to what was done by Roussopoulos (1993) and Park et al. (1994). Some of these results obtained at $\mathrm{Re} = 50$ are illustrated in Fig. 5(a) with reference to the C_D time trace. When the sensor is moved downstream, the compensator becomes slower and the amount of time required for the complete suppression of the vortex shedding gradually increases. Moreover for a sensor placement in the far-wake region with $x_s \geq 19$, the flow stabilisation cannot be achieved anymore and the controlled flow converges to a different limit cycle which is however characterised by a lower mean value of the drag coefficient. For practical purpose a measure T_s of the time required to suppress the vortex shedding can be introduced based on the residual amplitude of the drag coefficient fluctuations with respect to the base-flow value, i.e. $|C_D(t) - C_D^{(BF)}| \leq \epsilon$. In Fig. 5(b) the value of T_s computed for $\epsilon = 10^{-5}$ is plotted as a function of x_s: the stabilisation time shows a weak dependence on x_s up to $x_s \sim 10$ after which it rapidly increases. The same analysis has been performed by evaluating the total control

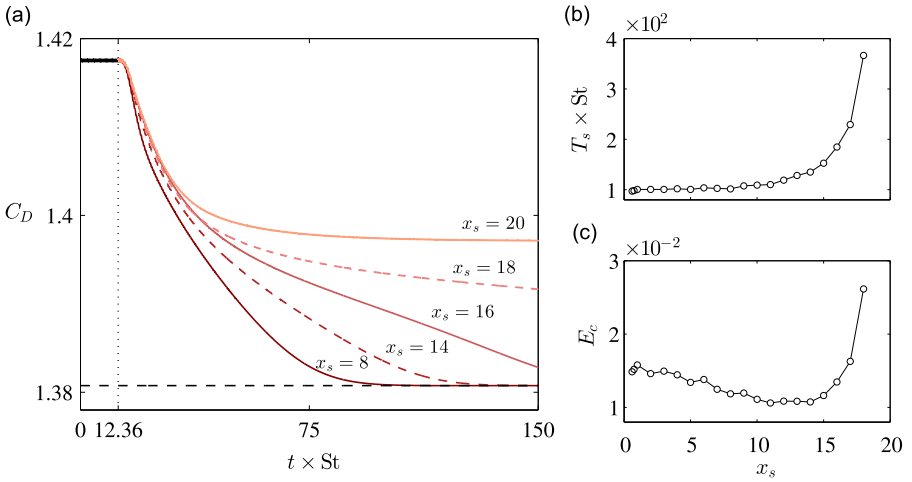

Fig. 5. Control of the flow past a circular cylinder at $\mathrm{Re} = 50$: performance of the SISO compensator for different positions x_s of the cross-stream velocity sensor along the symmetry line. (a) Time trace of the drag coefficient. Stabilisation time T_s (b) and total control energy E_c (c) as a function of x_s.

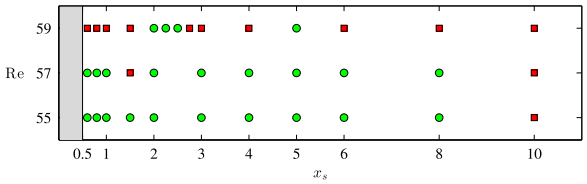

Fig. 6. Control of the flow past a circular cylinder using the SISO compensator. For each considered sensor position x_s and Reynolds number, the round marker indicates that complete flow stabilisation is achieved and the base-flow solution is restored, while the square marker indicates that the control is not able to completely suppress the vortex shedding, although it can reduce it.

energy $E_c = \int_0^{T_s} \varphi^2 dt$ spent to stabilise the flow which is plotted in Fig. 5(c). These latter results indicate that the value of E_c is reduced to a minimum when the sensor is approximately located within the range of $11 \leq x_s \leq 14$.

When increasing the Reynolds number up to $\mathrm{Re} = 59$, the range of effective sensor placements rapidly shrinks, both downstream and upstream. This is illustrated in Fig. 6 for $\mathrm{Re} = 55, 57$ and 59, indicating whether flow stabilisation is achieved or not for different locations of the sensor within 10 diameters from the cylinder centre. At $\mathrm{Re} = 59$ the cylinder vortex shedding is completely suppressed only when the sensor is located within the narrow interval of $2 \leq x_s \leq 2.5$ and in the neighbourhood of $x_s \approx 5$. When ineffective sensor placements are considered, different behaviours can be observed: two examples are illustrated in Fig. 7. For a sensor location very close to cylinder surface, namely at $x_s = 0.6$, the control action results in a weakened shedding cycle that is characterised by a lower value of $\langle C_D \rangle$, a reduced amplitude of the aerodynamic force fluctuations and approximately the same shedding frequency of the uncontrolled case with $\mathrm{St}_c = 0.137$ compared to

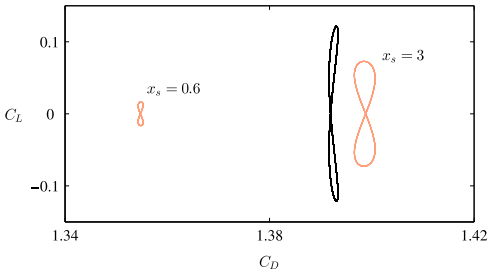

Fig. 7. Control of the flow past a circular cylinder at $\mathrm{Re} = 59$ using the SISO compensator: for both $x_s = 0.6$ and $x_s = 3$ the control action results in a different limit cycle ($\mathrm{St} = 0.1343$) compared to uncontrolled case (black line) with $\mathrm{St}_c = 0.1366$ for $x_s = 0.6$ and $\mathrm{St}_c = 0.1434$ for $x_s = 3$.

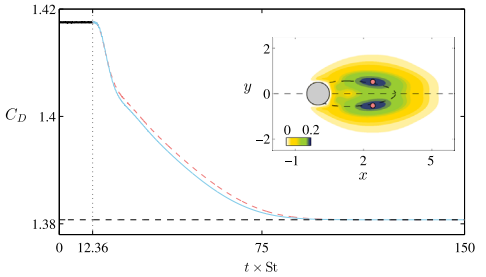

Fig. 8. MCE control of the flow past a circular cylinder at $\mathrm{Re} = 50$: performance of the MCE compensator using two velocity sensors located in the region of maximum structural sensitivity of the cylinder wake. The sensor positions (x_s, y_s) and $(x_s, -y_s)$ with $x_s = 2.406$ and $y_s = 0.52$ are indicated by the two round markers superposed to the wavemaker contour levels. Two different configurations are considered: the continuous line corresponds to the case where the signals $U(x_s, y_s)$ and $U(x_s, -y_s)$ are used for state estimation while the dashed line corresponds to the case where the signals $-V(x_s, y_s)$ and $V(x_s, -y_s)$ are employed instead.

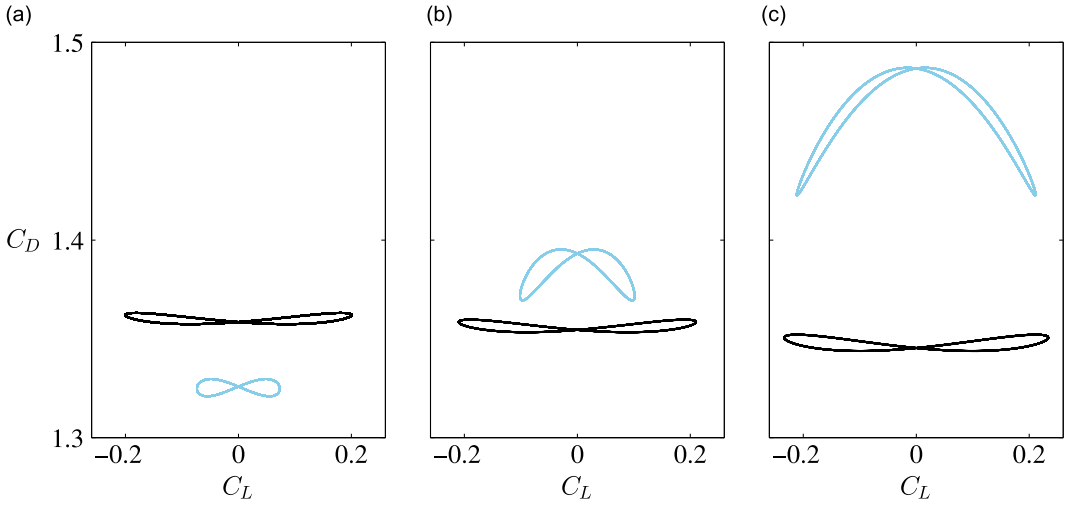

Fig. 9. Control of the flow past a circular cylinder: performance of the full-information feedback control above $\mathrm{Re} = 72$. (a) $\mathrm{Re} = 73$: $\mathrm{St} = 0.147$, $\mathrm{St}_c = 0.162$. (b) $\mathrm{Re} = 75$: $\mathrm{St} = 0.150$, $\mathrm{St}_c = 0.174$. (c) $\mathrm{Re} = 80$: $\mathrm{St} = 0.153$, $\mathrm{St}_c = 0.186$. For each case, both the uncontrolled (black line) and the controlled shedding cycle (blue line) are shown. (For interpretation of the references to color in this figure caption, the reader is referred to the web version of this article.)

the value of $St = 0.134$ that characterises the natural vortex shedding for the considered Reynolds number. By moving the sensor at $x_s = 3$ only the lift coefficient amplitude is reduced while both the mean drag coefficient and the shedding frequency are increased with $St_c = 0.143$. For $Re = 60$ the complete vortex-shedding suppression cannot be obtained for any streamwise position of the sensor, similar to what observed experimentally by Roussopoulos (1993) for $Re > 58$.

Sensor placement away from the symmetry line has also been tested. In their work, Chen and Rowley (2011) have shown that the region of maximum structural sensitivity, i.e. the so-called *wavemaker* (see Giannetti and Luchini, 2007) provides a good estimate for the optimal placement of actuators and sensors in a LQG-controlled system. Based on that result, two velocity sensors have been symmetrically placed within the wavemaker region where structural-sensitivity peaks are found, as shown in Fig. 8. More precisely two different configurations have been tested by probing at those spatial locations the U component of the velocity field in one case and the V component with opposite sign in the other case. Obtained results are illustrated in Fig. 8 by means of the time series of the drag coefficient. For both cases no substantial improvements are observed compared to the performance of the SISO compensator using a single V-sensor located along the x-axis.

Finally the effectiveness of the full-information regulator is investigated up to $Re = 80$. Differently from the compensator, the LQR control is able to stabilise the flow up to $Re = 72$. For $Re = 73$ the flow cannot be stabilised but the control action still results in a mitigation of the vortex shedding by reducing both the lift fluctuations and the drag mean value, as shown in Fig. 9(a). Further increasing the Reynolds numbers, Fig. 9(b) and 9(c), these beneficial effects are lost. Moreover the shedding frequency is substantially increased in the controlled case with $St_c = 0.186$ compared to $St = 0.153$ for $Re = 80$.

4. Discussion and conclusions

In this paper a linear feedback control of the cylinder wake is numerically investigated at low Reynolds numbers. The control actuation is performed by means of unsteady angular rotations of the cylinder surface and a single velocity sensor is used for the state estimation. A full-dimensional, MCE-LQG compensator of the linearised flow equations is designed and tested. Both feedback and observer gains have been efficiently computed by exploiting and further extending to the estimation problem the analytical results of Lauga and Bewley (2003). Thanks to this full-order approach, the control implementation results free from spill-over errors and can be used to investigate the best performance achievable on the actual flow by a reduced-order version of the considered compensator. However it is worthwhile to note that the considered MCE solution of the optimal control problem makes sense only for linearly unstable flows, such as fluid oscillators. In the case of flows of noise amplifier type, a similar analysis can be performed using the technique described by Semeraro et al. (2013), with reference to the general solution of the optimal control problem.

When the MCE-LQG compensator is applied to the unsteady flow past a circular cylinder at $Re = 50$ using located at $x_s < 19$, the vortex shedding is completely suppressed and the unstable steady base flow is finally restored. In particular, as the sensor position is varied from the near-wake to the far-wake region, two different behaviours are observed. On one hand, the time required to stabilise the flow gradually increases up to a limit where flow stabilisation is definitively lost. This behaviour can be ascribed to the nonlinear evolution of the vortex wake while moving downstream which may result in a phase-lag exceeding the maximum phase-margin of the closed-loop control within the linearised description. The stabilisation loss associated with a far-wake sensor placement was also described by Roussopoulos (1993): in his experiments a critical threshold of approximately 9 diameters from the cylinder centre was found when using a short-span cylinder model and for $Re = 65$. On the other hand, as the sensor is moved along the flow centreline, the amount of control energy spent to stabilise the flow is characterised by a small, lower plateau for $11 \le x_s \le 14$. These streamwise stations roughly correspond to the region where the highest values in the amplitude of the unstable mode are attained for $Re = 50$ (Giannetti and Luchini, 2007). Therefore it is worthwhile to note that the optimal placement for the "cheapest control", i.e. for the minimum value of the control energy, does not correspond to the "fastest" stabilising control configuration for which the sensor has to be placed in the near wake. As the Reynolds number is increased up to $Re = 59$ the range of effective sensor locations rapidly reduces to the narrow interval of $2 \le x_s \le 2.5$ except for the additional position $x_s \approx 5$ for which the vortex shedding is also completely suppressed. Similar results were obtained by Park et al. (1994) showing that for $Re = 60$ complete vortex-shedding suppression can be achieved only for a sensor position within the interval of $2.25 < x_s < 2.75$. This agreement seems to indicate that the effective sensor placement is rather independent from the adopted control strategy and actuation technique. However, differently from the previously cited works, in the present case no ad-hoc tuning of the control gain is required. Finally a further increase of the critical Reynolds number up to $Re = 72$ is achieved only when the full-information controller is used.

The relevant difference in terms of the critical Reynolds number between the MCE compensator ($Re \approx 59$) and the full-information controller ($Re \approx 72$) suggests that a substantial increase of the control performance on the actual nonlinear flow can be expected by introducing a nonlinear estimator in place of the linear optimal observer. Indeed the LQR control can be interpreted as the result of an ideal nonlinear compensator where the LQR design is combined with a perfect and infinitely fast nonlinear observer which is able to provide the exact flow state. A further increase of the control performance will therefore require to devise a fully nonlinear control strategy.

Obviously, the obtained results are limited to the considered flow configuration. Nonetheless, based on these results, it would be interesting to perform a similar analysis on a fully three-dimensional bluff-body flow in order to assess the potential of the linear optimal control on a more challenging and a more realistic flow configuration. In this latter case several different unstable modes are usually present and a multiple-input-multiple-output plant configuration has to be

considered. However in our approach no restriction has been introduced on the number of unstable modes as well as on the number of control inputs/outputs, thus making its application to three-dimensional cases almost straightforward. Such an analysis will be considered in a forthcoming work.

References

Ahuja, S., Rowley, C.W., 2010. Feedback control of unstable steady state of flow past a flat plate using reduced-order estimators. Journal of Fluid Mechanics 645, 447–478.

Amodei, L., Buchot, J.M., 2012. A stabilization algorithm of the Navier–Stokes equations based on algebraic Bernoulli equation. Numerical Linear Algebra with Applications 19, 700–727.

Barbagallo, A., Sipp, D., Schmid, P.J., 2009. Closed-loop control of an open cavity flow using reduced-order models. Journal of Fluid Mechanics 641, 1–50.

Bergmann, M., Cordier, L., Brancher, J.P., 2005. Optimal rotary control of the cylinder wake using proper orthogonal decomposition reduced-order model. Physics of Fluids 17, 1–21.

Bewley, T.R., Pralits, J.O., Luchini, P., 2007. Minimal-energy control feedback for stabilization of bluff-body wakes. In: Proceeding FEDSM 2002-31048. BBVIV5, Fifth Conference on Bluff Body Wakes and Vortex-Induced Vibrations, Bahia, Brazil.

Burl, J.B., 1998. Linear Optimal Control: H2 and H1 Methods, Addison-Wesley Longman Publishing Co., Inc., Boston, MA, USA. ISBN 020180868.

Chen, K.K., Rowley, C.W., 2011. h_2 optimal actuator and sensor placement in the linearised complex Ginzburg-Landau system. Journal of Fluid Mechanics 681, 241–260.

Choi, H., Jeon, W., Kim, J., 2008. Control of flow over bluff body. Annual Review of Fluid Mechanics 40, 113–139.

Curtain, R.F., Mikkola, K.M., Sasane, A., 2007. The Hilbert–Schmidt property of feedback operators. Journal of Mathematical Analysis and Applications 329, 1145–1160.

Davis, T.A., 2004. Algorithm 832: UMFPACK, an unsymmetric-pattern multifrontal method. ACM Transactions on Mathematical Software 30, 196–199.

Giannetti, F., Luchini, P., 2007. Structural sensitivity of the first instability of the cylinder wake. Journal of Fluid Mechanics 581, 167–197.

He, J.W., Glowinski, R., Metcalfe, R., Nordlandelr, A., Periaux, J., 2000. Active control and drag optimization for flow past a circular cylinder: I. oscillatory cylinder rotation. Journal of Computational Physics 163, 83–117.

Huerre, P., Rossi, M., 1998. Hydrodynamic instabilities in open flows. In: Godrèche, C., Manneville, P. (Eds.), Hydrodynamics and Nonlinear Instabilities, Cambridge University Press, Cambridge, UK, pp. 81–294.

Kang, S., Choi, H., Lee, S., 1999. Laminar flow past a rotating circular cylinder. Physics of Fluids 11, 3312.

Kim, J., Bewely, T.R., 2007. A linear system approach to flow control. Annual Review of Fluid Mechanics 39, 383–417.

Lauga, E., Bewley, T.R., 2003. The decay of stabilizability with Reynolds number in a linear model of spatially developing flows. Proceedings of the Royal Society of London A 459, 2077–2095.

Lehoucq, R.B., Sorensen, D.C., Yang, C., 1998. ARPACKUsers Guide. SIAM ed.

Lewis, F.L., Syrmos, V.L., 1995. Optimal Control. Wiley, New York.

Marquet, O., Sipp, D., Jacquin, L., 2008. Sensitivity analysis and passive control of cylinder flow. Journal of Fluid Mechanics 615, 221–252.

Meliga, P., Chomaz, J.M., 2011. An asymptotic expansion for the vortex-induced vibrations of a circular cylinder. Journal of Fluid Mechanics 671, 137–167.

Park, D.S., Ladd, D.M., Hendricks, E.W., 1994. Feedback control of von Kármán vortex shedding behind a circular cylinder at low Reynolds numbers. Physics of Fluids 6, 2390–2405.

Pralits, J.O., Brandt, L., Giannetti, F., 2010. Instability and sensitivity of the flow around a rotating circular cylinder. Journal of Fluid Mechanics 650, 1–24.

Pralits, J.O., Giannetti, F., Brandt, L., 2013. Three-dimensional instability of the flow around a rotating circular cylinder. Journal of Fluid Mechanics 730, 5–18.

Protas, B., 2004. Linear feedback stabilization of laminar vortex shedding based on a point vortex model. Physics of Fluids 16, 4473–4488.

Protas, B., Styczek, A., 2002. Optimal rotary control of the cylinder wake in the laminar regime. Physics of Fluids 14, 2073–2087.

Roussopoulos, K., 1993. Feedback control of vortex shedding at low Reynolds numbers. Journal of Fluid Mechanics 248, 267–296.

Semeraro, O., Pralits, J.O., Rowley, C.W., Henningson, D.S., 2013. Riccati-less approach for optimal control and estimation: an application to two-dimensional boundary layers. Journal of Fluid Mechanics 731, 394–417.

Sipp, D., Lebedev, A., 2007. Global stability of base and mean flows: a general approach and its applications to cylinder and open cavity flows. Journal of Fluid Mechanics 593, 333–358.

Stojković, D., Breuer, M., Durst, F., 2002. Effect of high rotation rates on the laminar flow around a circular cylinder. Physics of Fluids 14, 3160.